Text and references accompanying Nevada Bureau of Mines and Geology Map 187

Geologic Map of the Terrill Mountains Quadrangle, Churchill and Mineral Counties, Nevada

by

Chad W. Carlson

Nevada Bureau of Mines and Geology, University of Nevada, Reno

2018

ABSTRACT

Positioned between the Sierra Nevada microplate and Basin and Range Province, the Walker Lane accommodates ~20% of the dextral motion between the North American and Pacific plates. This motion is primarily accommodated on northwest-striking dextral and east-northeast- to east-striking sinistral fault systems. The Terrill Mountains lie at the northern terminus of dextral faults translating crustal blocks of the central Walker Lane and at the southeastern edge of sinistral faults accommodating oroclinal flexure and clockwise-rotation of blocks in the northern Walker Lane. As the mechanisms of strain transfer between these disparate fault systems are poorly understood, the thick Oligocene to late Miocene volcanic strata of the Terrill Mountains make it an ideal site for studying the transfer of strain between regions undergoing differing styles of deformation and yet both accommodating dextral shear. Detailed geologic mapping of the Terrill Mountains 7.5-minute quadrangle was completed to help elucidate the Neogene styles of, and changes in, strain accommodation for this region of the Walker Lane. Detailed geologic mapping of the Terrill Mountains quadrangle greatly enhanced understanding of the stratigraphic and structural framework of the area.

The Tertiary strata include at least nine individual late Oligocene ash-flow tuffs disconformably overlain by middle Miocene lavas and volcaniclastic rock. Several ash-flow tuffs, not previously identified in the Terrill Mountains, were geochronologically correlated to regionally extensive units in the western Great Basin. These include the ~25.4 Ma Nine Hill Tuff, the ~25.1 Ma tuff of Gabbs Valley, and the ~23.3 Ma tuff of Toiyabe. Previously inferred as a low-angle normal detachment fault, a distinct and localized ~23 Ma paleosol is preserved below the tuff of Toiyabe. This paleosol provides an important marker bed, which is right-laterally separated ~6 km across the Benton Spring fault system that bounds the northeast flank of the Terrill Mountains. Strain at the northern part of the Terrill Mountains appears to be transferred from predominatly northwest-striking dextral faults to systems of approximately east-striking sinistral faults and clockwise flexure of the northernmost part of the range. The northern Terrill Mountains may represent a localized region of strain transfer analogous to the greater transition between the central and northern Walker Lane. The detailed mapping of the Terrill Mountains quadrangle, initiated through the EDMAP component of the National Cooperative Geologic Mapping Program, has provided a firm foundation for future geologic mapping, structural analysis, and paleomagnetic studies in the region.

INTRODUCTION

Positioned between the Sierra Nevada microplate and Basin and Range Province, the Walker Lane accommodates ~20% of the dextral motion between the North American and Pacific plates in structural domains of discontinuous systems of dextral, sinistral, and normal faults (fig. 1; e.g., Stewart 1988, Faulds and Henry, 2008). The Pyramid Lake and Walker Lake structural domains in the northern and central Walker Lane, respectively, consist of a series of left-stepping, en echelon, NW-striking dextral faults, separated by east-northeast-striking sinistral faults and a large oroclinal flexure in the Carson structural domain (fig. 1; e.g., Faulds and Perkins, 2007; Faulds and Henry, 2008). Although significant progress has been made in recent years in understanding the evolution (e.g., Cashman and Fontaine, 2000; Oldow et al., 2001; Briggs and Wesnousky, 2004; Faulds et al., 2005; Faulds and Henry, 2008; Lee et al., 2009; Carlson et al., 2013) and recent styles of Walker Lane strain accommodation (Wesnousky, 2005; Wesnousky et al., 2012; Bormann et al., 2016), the kinematic links and mechanisms of strain transfer between these disparate fault systems are poorly understood.

To address some of the important scientific and societal issues at the transition between the northern and central Walker Lane, detailed geologic mapping of the 7.5-minute Terrill Mountains quadrangle was completed. This quadrangle is strategically situated at the inferred northern continuation of northwest-striking dextral faults of the

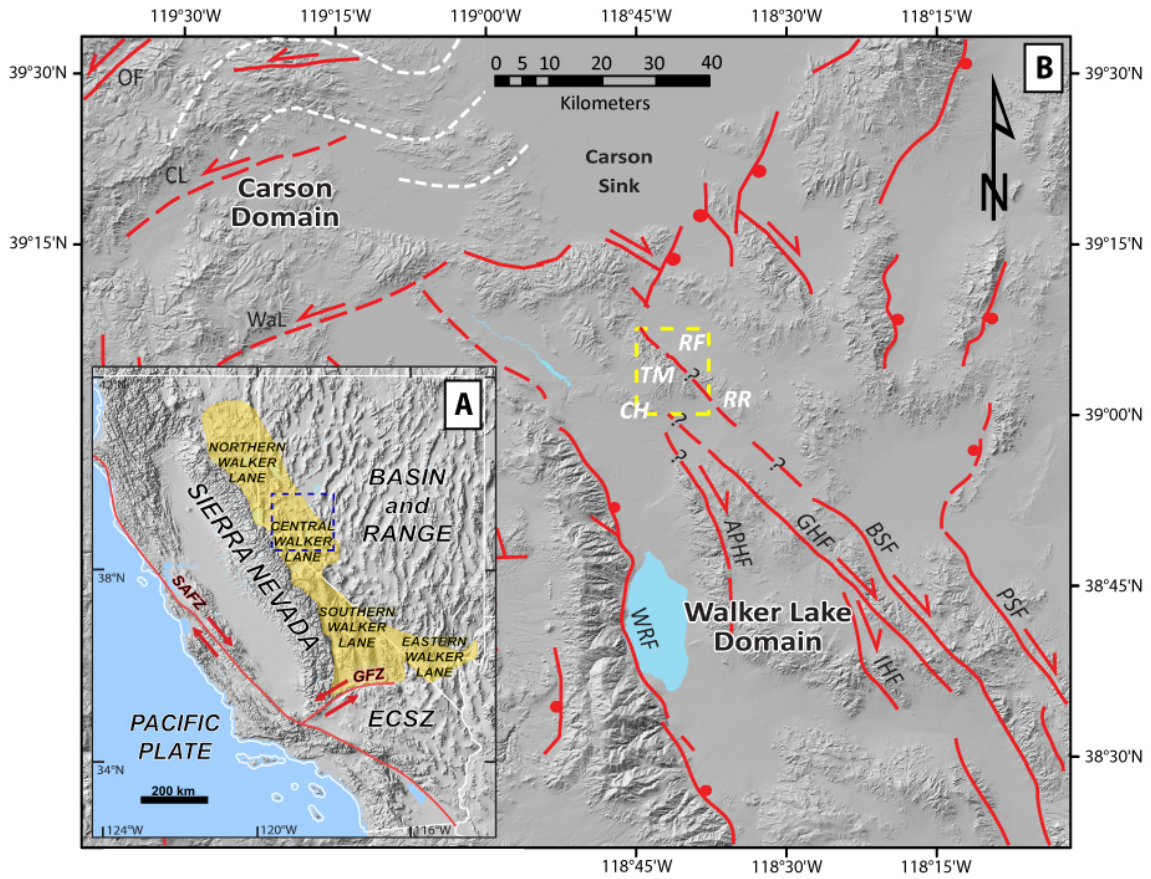

Figure 1. A: Shaded-relief map depicting a part of western North America, modified from Carlson et al. (2013). Walker Lane shaded in yellow and divided into northern, central, southern and eastern parts. ECSZ, Eastern California Shear Zone; GFZ, Garlock fault zone; SAFZ, San Andreas fault zone. Blue dashed box shows approximate location of figure 1B. B: Shaded-relief map of the Walker Lake (central Walker Lane) and Carson (northern Walker Lane) domains. Yellow dashed polygon shows location of Terrill Mountains quadrangle. Major faults and lineaments in the central and northern Walker Lane, modified from Faulds and Henry (2008). Regional faults: APHF, Agai Pah Hills fault; BSF, Benton Spring fault; CL, Carson lineament; GHF, Gumdrop Hills fault; IHF, Indian Head fault; OF, Olinghouse fault; PSF, Petrified Spring fault; Wal, Wabuska lineament; WRF, Wassuk Range frontal fault. White dashed lines denote orocline of Faulds and Henry (2008). Physiographic regions: CH, Calico Hills; RF, Rawhide Flats; RR, Red Ridge; TM, Terrill Mountains.

central Walker Lane (fig. 1; e.g., Ekren and Byers, 1984; Wesnousky, 2005; Faulds and Henry, 2008). These dextral fault systems transfer strain to left-lateral faults and oroclinal flexure accommodating clockwise vertical-axis rotation of crustal blocks in the southeastern part of the northern Walker Lane (Cashman and Fontaine, 2000; Faulds and Perkins, 2007).

SUMMARY OF WORK PERFORMED

The Terrill Mountains 7.5-minute quadrangle was mapped during the summer and fall of 2013, with some additional mapping completed during the early part of 2014. Geologic data collected in the field were mapped on 1:24,000-scale, color, stereographic air photos. Petrographic analysis of thin sections and mineralogical descriptions of collected hand samples were used for correlation and detailed description of mapped geologic units. Field data were compiled and digitized using VR software by Cardinal Systems to produce a three-dimensional model of individual stereo-photo pairs in the map area. The digitized field map was then exported to ArcGIS for final cartographic production and completion of cross sections. A preliminary geologic map of the Terrill Mountains quadrangle was published as an Open-File Report by the Nevada Bureau of Mines and Geology (Carlson, 2014).

Seven geochronological samples were analyzed by the New Mexico Geochronology Research Laboratory in the summer of 2016. $^{40}Ar/^{39}Ar$ dates were obtained for three ash-flow tuffs, an early Miocene intrusion, an early Miocene lava, and a late Miocene lava (table 1). Results from an additional sample from a latest Oligocene to earliest Miocene lava returned an anonymously old age and is not included on the final map or discussed further (see Appendix A). Single crystal analyses of sanidine were completed on the ash-flow tuffs. The dates and composition of these units indicate correlations with the tuff of Toiyabe, tuff of Gabbs, and Nine Hill Tuff (e.g., Henry and John, 2013; table 1).

Table 1. Radiogenic Ages ($^{40}Ar/^{39}Ar$)

Sample ID	Map Unit	Mineral Dated	Age (Ma)	±2 sigma	Latitude (NAD 83)	Longitude (NAD 83)	Source
CC15-021-3	Tb	groundmass concentrate	5.79	0.06	N39.02860°	W118.67542°	This Study
MBK06-4	$Tbka_2$	plagioclase	19.15	0.23	N39.06489°	W118.70792°	This Study
CC15-021-1	Ti	plagioclase	22.67	0.15	N39.05908°	W118.68935°	This Study
NTM-093-1	Ttt	sanidine	23.29	0.02	N39.10677°	W118.74935°	This Study
STM04-2	Tgv	sanidine	24.95	0.02	N39.03399°	W118.69279°	This Study
PMA01-2	Tnh	sanidine	25.44	0.02	N39.10161°	W118.72333°	This Study

Note: Age determinations completed by the New Mexico Geochronology Research Laboratory. See Appendix A for techniques, analytical data, and incremental release spectra.
Map units: Tb, basaltic lavas; $Tbka_2$, younger andesitic lavas of Brown Knob; Ti, plagioclase hornblende intrusions, dikes, and sills; Ttt, tuff of Toiyabe; Tgv, tuff of Gabbs Valley; Tnh, Nine Hill Tuff.

Step-heated, multigrain plagioclase separates for the early Miocene lava and intrusion and a groundmass concentrate for the late Miocene lava yielded slightly disturbed age spectra (Appendix A). Calculated weighted mean ages are derived from the flattest and most radiogenic parts of the age spectra (table 1). $^{40}Ar/^{39}Ar$ ages and locations are included on the map of the Terrill Mountains quadrangle.

STRATIGRAPHIC FRAMEWORK

Bedrock

The bedrock exposures in the map area consist of Tertiary volcanic and sedimentary rocks resting nonconformably on Mesozoic plutonic rocks. The Mesozoic rocks crop out in the northwest part of the quadrangle in the footwall of the Benton Spring fault bounding the northeast flank of the Terrill Mountains. Two Mesozoic units of gabbro and quartz diorite were identified in the quadrangle, with relative ages based on previous work in the region (e.g., Hardyman et al., 1992; Hinz et al., 2010). Cross-cutting relationships or unit contacts between 'KJg' and 'Jqd' were not observed in the map area.

At least nine Oligocene ash-flow tuffs were mapped in the Terrill Mountains quadrangle. The oldest identified ash-flow tuff is the Guild Mine Member of the Mickey Pass Tuff (Tmp). The Guild Mine Member was identified through phenocryst assemblages and paleomagnetic correlation (Geissman et al., 1982; Carlson, 2017b). The Mickey Pass Tuff nonconformably overlies Mesozoic basement in the northwest part of the quadrangle and was deposited on an irregular erosion surface. Thus, the attitudes of compaction foliations in the tuff vary widely, as they generally subparallel the erosional surface. The younger Weed Heights Member of the Mickey Pass Tuff was not observed in the quadrangle. The Nine Hill Tuff rests disconformably on the Mickey Pass Tuff in the northern Terrill Mountains. Single-crystal $^{40}Ar/^{39}Ar$ analyses of sanidine (n=12) resulted in a weighted mean age of 25.44±0.02 Ma (PMA01-2; table 1). A localized breccia consisting of clasts of Mickey Pass Tuff was deposited over the Mickey Pass Tuff. The subangular to subrounded clasts range in size from coarse sands to boulders. This breccia is similar to a breccia mapped in the Nine Hill paleovalley approximately 80 km to the west (Henry and Faulds, 2010). In contrast to stratigraphy in the Nine Hill paleovalley, this breccia was not observed stratigraphically below the Nine Hill Tuff in the Terrill Mountains region. An unidentified ash-flow tuff overlies the Nine Hill Tuff and Mickey Pass Tuff in the central and northern Terrill Mountains, respectively. This 'unknown tuff 2' (Ttu_2) is readily distinguishable in the map area by an abundance of lithic clasts composing up to ~20% of the unit in some locations.

Conformably above 'Ttu_2' in the Terrill Mountains is a poorly to moderately welded and undivided section of ash-flow tuffs that may consist of multiple cooling breaks and has potential for division into separate ash-flow tuffs with further study. Part, if not all, of a tuff identified as 'unknown tuff 3' (Ttu_3) in the central and southern Terrill Mountains may correlate with the tuff of Elevenmile Canyon (e.g., Henry and John, 2013) in the northern Terrill Mountains. The phenocryst assemblage of the tuff of Elevenmile Canyon mapped in the Terrill Mountains is consistent with the tuff of Elevenmile Canyon studied in the nearby Stillwater Range (e.g., relatively-high biotite percentage; John, 1995). Stratigraphically below the basal-surge of the tuff of Elevenmile Canyon is a relatively thin (~5–10 m thick) ash-flow tuff vitrophyre (Ttv) exposed in the northern Terrill Mountains. Though not present in the southern and central Terrill Mountains, this vitrophyre may correlate to an unidentified, less-densely welded, lower section of 'Ttu_3' in the map region.

The tuff of Gabbs Valley crops out extensively throughout most of the quadrangle as a distinct, widely distributed, and erosion-resistant stratigraphic unit. Although relatively sparse and discontinuous in the northern Terrill Mountains, the tuff of Gabbs Valley can be used as a distinctive stratigraphic horizon for quick identification of relatively younger and older Oligocene strata in the Terrill

Mountains and surrounding region. Previously mapped as the Nine Hill Tuff in the central and southern Terrill Mountains (Carlson, 2014), based on similar phenocryst assemblage and stratigraphic position, the tuff of Gabbs Valley records a distinct paleomagnetic remanent magnetization of reverse polarity and low inclination to the south-southeast (Carlson, 2017b). This direction is distinct from the normal polarity, northwest-trending declination, and steeper inclination of the Nine Hill Tuff (Deino, 1985; Faulds et al., 2004), and correlates to a paleomagnetic direction for the tuff of Clipper Gap (Gromme et al., 1972). Single-crystal $^{40}Ar/^{39}Ar$ analyses of sanidine (n=11) from a sample of the tuff of Gabbs Valley resulted in a weighted mean age of 24.95±0.02 Ma (STM04-2; table 1). This result is consistent with previously determined ages for the tuff of Gabbs Valley (e.g., Henry and John, 2013). A discontinuous and relatively thin 'unknown tuff 4' (Ttu_4) crops out conformably above the tuff of Gabbs Valley in the southern half of the Terrill Mountains quadrangle. An 'unknown tuff 5' (Ttu_5) disconformably overlies the tuff of Gabbs Valley where 'unknown tuff 4' does not crop out, and is presently not correlated to any ash-flow tuff identified in the region.

Figure 2. Outcrop of volcaniclastic conglomerate (Tvc) in the northern Terrill Mountains. Hammer is ~35 cm long for scale.

The tuff of Toiyabe (Ttt) is correlated with the Santiago Canyon Tuff and is the youngest Oligocene ash-flow tuff observed in the western Great Basin (Henry and John, 2013). Single-crystal $^{40}Ar/^{39}Ar$ analyses of sanidine (n=10) resulted in a weighted mean age of 23.29±0.02 Ma (NTM-093-1; table 1). The contact between the tuff of Toiyabe and 'unknown tuff 5' stratigraphically below was previously inferred as a low-angle normal detachment fault (Hardyman et al., 1992). On the basis of both a lack of deformation along the inferred fault plane and varying levels of apparent soil development along this contact (see unit description), it was concluded that this contact is likely a soil and weathering horizon rather than a detachment fault. A distinct and localized reddish-brown clay-rich horizon along parts of this contact is inferred to be a paleosol formed on the erosional surface of 'unknown tuff 5'. During this same depositional hiatus between 'unknown tuff 5' and the tuff of Toiyabe, the oldest lavas and sedimentary rocks observed in the area were deposited in the northern Terrill Mountains. These distinct basaltic lavas contain large, platey, plagioclase phenocrysts and are intercalated with volcaniclastic conglomerates and sandstones (Tvc) in the northwest corner of the quadrangle. These conglomerates are interpreted as volcanic debris flows based on poorly-sorted, matrix-supported, angular-subangular clasts of predominately volcanic rocks ranging from pebbles to boulders (fig. 2).

Across the central and southern Terrill Mountains are lavas and clastic sediments of Brown Knob, named for the topographic high where the thickest exposed section of these units resides. Brown Knob consists of an older section of basaltic lavas ($Tbka_1$) and younger section of andesitic lavas ($Tbka_2$) separated by volcaniclastic rocks including conglomerates, breccias, and moderately- to poorly-indurated, finer-grained gravels and sands (Tbkc). Several volcanic breccias that make up part of 'Tbkc' consist of poorly-sorted, angular clasts of andesitic volcanic rock within a fine-grained and ash matrix of similar composition (fig. 3).

Figure 3. Outcrop of volcanic breccia in the clastic rocks of Brown Knob (Tbkc) in the Terrill Mountains. Hammer is ~35 cm long for scale.

The breccias are interpreted as block and ash flows and may be related to, or very slightly predate, the overlying andesitic lavas of Brown Knob. These lavas and volcaniclastic sedimentary rocks disconformably overlie Oligocene ash-flow tuffs in most of the quadrangle. Step-heated, multigrain $^{40}Ar/^{39}Ar$ analyses (n=10) of plagioclase collected from the stratigraphically highest flow preserved on Brown Knob yielded a plateau age of 19.15±0.23 Ma (MBK06-4; table 1). The youngest basaltic lavas (Tb) crop out in the southern part of the quadrangle and rest in angular unconformity on older rock types. Step-heated $^{40}Ar/^{39}Ar$ analyses of groundmass concentrates collected from the base of these young basaltic lavas resulted in a plateau age of 5.79±0.06 Ma (CC15-021-3; table 1).

Intrusions in the Terrill Mountains quadrangle vary in composition from mafic to felsic (e.g., Tbi, Thai, Tdi, and Tri). Most intrusions are relatively small and isolated bodies. However, the plagioclase-hornblende dacite (Ti) crops out extensively in the study area, forming dikes, sills, and irregular-shaped massive bodies. Sills of Ti are commonly emplaced within the more poorly-welded ash-flow tuffs (e.g., Ttu_3 and Ttu_5). The 'Ti' intrusions are most abundant in the central-northern Terrill Mountains, where poorly-welded tuffs are more widespread. Step-heated, multigrain $^{40}Ar/^{39}Ar$ analysis of plagioclase from a large intrusive body of 'Ti' in the central Terrill Mountains yielded a plateau age of 22.67±0.15 Ma (CC15-021-1; table 1). Most of the intrusions cut early Miocene units in the study area (e.g., Tbkc). The basaltic intrusion (Tbi) is only observed to cut Oligocene ash-flow tuffs in the Terrill Mountains.

Quaternary Sediments

Quaternary deposits in the Terrill Mountains quadrangle consist of alluvial (coarse sands to gravels), lacustrine (silts, fine sands, and gravels), and eolian (fine to medium sands). The oldest alluvium included in the Quaternary units consists of alluvial-fan sediments (QTaf) that may range in age from late Pliocene (?) to late Miocene. These fans are locally tilted gently and contrast with essentially flat-lying younger fans. An east-dipping fan (28°) observed in the southwest corner of the map, west of an inferred continuation of the Gumdrop Hills fault (e.g, Hardyman et al., 1992) may be structurally equivalent to eastern-tilted units along the northeast flank of Terrill Mountains, adjacent to the trace of the Benton Spring fault. This notable dip magnitude, consistent with dips in Oligocene ash-flow tuffs to the south, lend to an interpreted late Miocene oldest age.

Inset into 'QTaf' are late Pleistocene alluvial fans (Qaf_1). Late Pleistocene fans are mapped along the flanks of the southern and northeastern Terrill Mountains and are commonly veneered with silts, fine sands, and irregular deposits of well-rounded, coarse gravel and sand that form curvilinear bars that follow topographic contour. Small (~5–10 mm) gastropod shells are locally found within these finer-grained sediments. In addition to 'Qaf_1', silts and fine sand locally form a veneer on 'Tbp' exposures in the hanging wall of the fault bounding the northeast flank of the Terrill Mountains. Similar in characteristic to the veneers of 'Qaf_1', late Pleistocene silt and fine sand are commonly in the lowest topographic areas of the quadrangle, with some deposits mapped up to the elevation of the Lake Lahontan highstand (e.g., Reheis, 1999), where not removed through erosion or obscured by younger alluvial fans. These fine-grained sediments and bars of rounded gravel and sand are interpreted as lacustrine deposits (Ql).

Inset into Qaf_1 are post-lacustrine (i.e., latest Pleistocene to Holocene) alluvial fans (Qaf_2). Qaf_1 deposits both drape over and are inset against lacustrine sediments. The youngest alluvial-fan deposits (Qafy) are inset against older fan deposits and are active depositional surfaces in parts of the quadrangle. The youngest Quaternary units consist of recent rock fall deposits (Qco), recent alluvium in active washes (Qa and Qay), ephemeral playas (Qp), and anthropogenically modified surfaces (Qx).

In addition, three Quaternary eolian units crop out within the quadrangle. The oldest inferred eolian deposits (Qafe) commonly form expansive sheets mantling the oldest alluvial fan and bedrock surfaces. These surfaces consist of fine sand with isolated, and potentially remnant, sand dunes in some locations. Isolated eolian deposits (Qe) are locally deposited on steep slopes. The youngest eolian deposits are sand dunes (Qed) in the lowest topographic regions (e.g., Rawhide Flats).

STRUCTURAL FRAMEWORK

The Terrill Mountains quadrangle is characterized by northwest-striking dextral-normal oblique faults that are inferred to accommodate both translation and southwest tilting of fault-bounded blocks. Initiation of these major faults and significant tilting of the Terrill Mountains may have begun in the early Miocene, with most of the deformation occurring post-middle to late Miocene based on similar dip magnitudes in Oligocene ash-flow tuffs and early to middle Miocene units. Positioned at the northern end of major northwest-striking dextral fault systems of the central Walker Lane (fig. 1), the northernmost part of the Benton Spring fault system has been inferred to bound the northeast flank of the Terrill Mountains (e.g., Ekren and Byers, 1984; Hardyman et al., 1992). Outcrops of a distinct and localized late Oligocene paleosol in the map area are offset with ~6 km of right-lateral separation across this fault. This offset paleosol is observed in the southeast range front of the central Terrill Mountains, at the eastern end of cross section line B–B'; and at the southern part of the east edge of the map, within the north end of the inferred dextrally-offset Red Ridge crustal block (e.g., Hardyman et al., 1992; Carlson, 2017a). Similar northwestern continuations of the Gumdrop Hills and/or Agai Pah Hills faults have been inferred extending into the valley between the Terrill Mountains and Calico Hills in the southwest corner of the quadrangle (fig. 1; e.g., Ekren and Byers, 1984; Hardyman, et al., 1992; Henry and Faulds, 2008). These central Walker Lane fault systems are consistent with the position and strike of northwest-striking, dextral normal oblique faults in the Terrill Mountains region. The fault between the Terrill Mountains and Calico Hills is very linear and may accommodate greater magnitudes of strike-slip motion than evident in the Terrill Mountains quadrangle. Between the inferred northern continuations of these major central Walker Lane fault systems are multiple northwest-striking dextral oblique faults that accommodate smaller magnitudes of slip within the central part of the Terrill Mountains. Opposite tilt directions of Tertiary strata accommodated on these faults along the northeast range-front and those southwest of the crest of the Terrill Mountains form an extensional syncline (see cross section B–B'). The inferred right-lateral separation on the Benton Spring fault

accommodated translation of the Terrill Mountains and Red Ridge structural blocks to the northwest and southeast, respectively, relative to one another (fig. 1). The southern segment of the Benton Spring fault appears to accommodate minimal normal displacement, yet the northernmost Terrill Mountains range-bounding segment of the fault has significant apparent vertical displacement with Mesozoic basement rocks exposed in the footwall and Quaternary basin-fill sediments dominating much of the hanging wall. Additionally, in contrast to the relatively linear trace of major strike-slip faults in the region, the northernmost trace of the Benton Spring fault bounding the Terrill Mountains is more curvilinear. Combined, these relationships may reflect strain partitioning to unrecognized, dextral faults within the Quaternary sediments along the western part of Rawhide Flats to the northeast (fig. 1).

Faults within the northern and southern Terrill Mountains differ from the major northwest-striking dextral faults in the study area. At the northernmost Terrill Mountains, strain is accommodated on east- to northeast-striking left-lateral oblique fault systems. The more northeasterly striking left-lateral faults terminate into one of the major east-west striking faults. The northeasterly striking faults, although having accommodated less total offset than the east-west striking faults, appear to have a greater component of dip-slip motion. Also, the northernmost Terrill Mountains appear to have undergone clockwise flexure. This flexure is evident in a change in dip directions on the western flank of the range. Dip directions rotate from southwest in the central Terrill Mountains to northwest toward the northern end of the range. In contrast, the southeastern Terrill Mountains are characterized by several north-northeast-striking, east-southeast-dipping, normal faults. These faults appear to terminate at the Benton Spring fault and may kinematically link major northwest-striking dextral faults in the study region. The attitudes of these normal and right-lateral oblique faults are consistent with syntectonic fault systems in a transtensional setting, with maximum and minimal principal strain axes oriented approximately east-west and north-south, respectively.

Fault scarps are observed in alluvial-fan units QTaf and Qaf_1 along the Benton Spring fault and several normal faults in the southern part of the Terrill Mountains. Scarps in Qaf_1 demonstrate that faulting has continued into at least the late Pleistocene based on late Pleistocene lake deposits, which overly these alluvial fans. These fault scarps are located upslope from the Lake Lahontan highstand (Reheis, 1999) and are not observed in the lake deposits themselves. Normal fault offsets are preserved as ~1–2 m scarps in several locations in the study area. Observed dextral offsets are less obvious and limited to the Benton Spring fault trace along the northeast range-front of the Terrill Mountains as deflected drainages and channel margins. Faults in the Terrill Mountains quadrangle are not observed cutting younger alluvial fans (e.g., Qaf_2 and Qafy) or lacustrine sediments (e.g., Ql).

SUMMARY OF FINDINGS

Upon completion of detailed geologic mapping of the Terrill Mountains quadrangle, several important observations were noted for continued study. Preliminary results identified ash-flow tuffs not previously noted in the Terrill Mountains (e.g., Nine Hill Tuff, tuff of Gabbs Valley; Henry and John, 2013). Ongoing correlations through additional petrographic analysis, geochronology, and paleomagnetic study will aid in the robust identification of all ash-flow tuffs, not only in the quadrangle but in the greater region.

The magnitude (~6 km) of right-lateral separation observed on the Benton Spring fault bounding the northeast flank of the Terrill Mountains is consistent with documented dextral displacement on the fault to the southeast (e.g., Ekren and Byers, 1986). Strain in the northern Terrill Mountains appears to be transferred from predominately northwest-striking dextral faults to systems of approximately east-striking sinistral faults and clockwise flexure of the northernmost range. The northern Terrill Mountains may represent a localized region of strain transfer analogous to the greater transition between the central and northern Walker Lane. In contrast, the southern Terrill Mountains are characterized by several north-northeast-striking normal faults that may kinematically link major northwest-striking dextral faults in the study region.

Thus, the geologic mapping of the Terrill Mountains quadrangle has elucidated an important region at the transition between the northern and central Walker Lane and provided an excellent foundation for further studies in the region. Additional mapping completed by Carlson (2017a) in the southern half of the Red Ridge quadrangle directly east has complemented the mapping of the Terrill Mountains and advanced understanding of strain accommodation and transfer at the northern termination of the Benton Spring fault and central Walker Lane.

DESCRIPTION OF MAP UNITS

Quaternary Deposits

Anthropogenic deposits

Qx Anthropogenic deposits and altered surfaces (Historical) Areas extensively disturbed and/or obscuring geologic units by anthropogenic activities (e.g., mine dumps).

Eolian deposits

Qe Eolian sand deposits (Holocene) Deposits of moderately to well-sorted, medium- to fine-grained sand that overlie bedrock and oldest alluvial-fan units. Deposits are not regionally extensive and primarily located on steep slopes; commonly not more than ~1–2 m thick.

Qed Sand dunes (Holocene) Deposits of well-sorted, medium- to fine-grained sand that form irregular, and locally elongate, dune fields in the topographically lowest and flattest areas. The largest dune field is in Rawhide Flats in the northeast part of the quadrangle. Dune heights range from ~1 to 5 m.

Qafe Alluvial-fan deposits with veneer of sands and silts (Holocene to early Pleistocene) Veneers (< 0.5 m thick) of moderately sorted medium- to fine-grained sand and silt deposited on older fan surfaces (e.g., QTaf). Most large deposits overlie broad southwest-dipping surfaces on the southwestern slope of the Terrill Mountains.

Alluvial deposits

Qay Deposits in recently active washes (Holocene) Youngest, poorly sorted, alluvial sediments, ranging in size from boulders to silt and deposited in intermittent washes and ephemeral stream beds; commonly less than ~1 m thick.

Qa Alluvium (Holocene) Short-travelled moderately sorted sands to cobbles deposited on moderately to gently sloped surfaces; commonly less than ~1 m thick.

Qa/Ql Alluvial deposits over lacustrine deposits (Holocene) Veneers of alluvium deposited on late Pleistocene lacustrine deposits; commonly less than ~1 m thick.

Qco Colluvium (Holocene) Veneer of angular and poorly sorted cobble to boulder clasts deposited on steep slopes, mainly developed below outcrops of Tb in the southern Terrill Mountains; mapped deposits obscure underlying units; commonly ~1–2 m thick.

Lacustrine and playa deposits

Qp Playa deposits (Holocene) Fine-grained sediments (fine sand-silt/clay) deposited from ephemeral lakes in closed depressions, primarily in northeast part of quadrangle (e.g., Rawhide Flats); commonly less than ~1 m thick.

Ql Lacustrine deposits (late Pleistocene) Undivided offshore, nearshore, and onshore deposits of fine sand, silt and mud, gravel bars, and cemented, well-rounded sands, pebbles, and cobbles. Deposits range in thickness from <~0.5 m of onshore deposits, to a few to tens of meters of near- and off-shore deposits.

Ql/Qaf$_1$ Lacustrine deposits over alluvial-fan deposits (late Pleistocene) Veneers of late Pleistocene lacustrine fine sand and silt deposited on older late Pleistocene alluvial fans; commonly less than ~1 m thick.

Ql/Tbp Lacustrine deposits on plagioclase basalts (late Pleistocene) Veneers of late Pleistocene lacustrine silt and fine sand resting on plagioclase basalts in the hanging wall of the fault bounding the northeast flank of the Terrill Mountains; commonly less than ~1 m thick.

Alluvial-fan deposits

Qafy Recently active alluvial-fan deposits (Holocene) Young alluvial-fan deposits consisting of poorly sorted sands and subangular pebble to cobble, and locally boulder, gravels inset into older alluvial-fan units; commonly less than ~1 m thick.

Qaf$_2$ Alluvial-fan deposits (Holocene) Alluvial-fan deposits consisting of poorly sorted sands and subangular pebble to cobble, and locally boulder, gravels inset into older alluvial-fan units. Surfaces have better developed desert pavement and varnish development than Qafy and lack onlapping late Pleistocene lacustrine sediments; commonly a few- to several- meters-thick.

Qaf$_1$ Alluvial-fan deposits (late Pleistocene) Alluvial-fan deposits consisting of poorly sorted sands and subangular pebble to cobble, and locally boulder, gravels inset into older alluvial-fan units; commonly a few- to several- meters-thick. Fan surfaces are commonly more dissected and have better developed desert pavement and varnish development than Qaf$_2$. Commonly onlapped by late Pleistocene lacustrine sediments below the late Pleistocene Lake Lahontan highstand.

Qaf Alluvial-fan deposits, undivided (Holocene to late Pleistocene) Alluvial-fan deposits consisting of poorly sorted sands and subangular pebble to cobble, and locally boulder, gravels; commonly a few to tens of meters thick. Unit older than young alluvial fans (i.e., Qafy) but lacks field relations for relative age determination.

QTaf Alluvial-fan deposits (middle Pleistocene to late Miocene) Alluvial-fan deposits consisting of poorly sorted sands and subangular pebble to cobble, and locally boulder, gravels; commonly a few to tens of meters thick. Surfaces display well-developed desert pavement and varnish. Topographically higher than other alluvial fans and locally gently tilted in contrast to younger, essentially subhorizontal alluvial fans. Fan deposits range from a few to tens of meters thick.

Tertiary Rocks

Oligocene–Miocene volcanic and sedimentary rocks

Tb Basaltic lavas (late Miocene) Youngest aphanitic mafic lavas, less commonly vesicular than older mapped basalts. Intergranular groundmass of ~90–95% interstitial plagioclase laths (~0.1–0.3 mm), with ~5–10% olivine, commonly altered to iddingsite (~0.1–0.5 mm). Outcrops typically display platy joints along foliation planes, locally becoming undulatory at the base of flow where exposed. Crops out in the south and southeast parts of the quadrangle; commonly ~20–30 m thick. Age: 5.79±0.06 Ma (^{40}Ar/^{39}Ar, this study).

Tbku Lavas and clastic rocks of Brown Knob, undivided (early Miocene) Named for the highest peak in the Terrill Mountains, Brown Knob consists of basaltic to andesitic lavas and intercalated sedimentary rocks. Mapped

as undivided in parts of the quadrangle, where exposures are poor or less distinct.

Tbka$_2$ Younger andesitic lavas of Brown Knob (early Miocene) Multiple flows of porphyritic andesitic lava with interstitial plagioclase groundmass ranging from light to medium gray and pinkish-gray; contains phenocrysts of euhedral to subhedral labradorite (~10–15%, 1–3 mm long), orthopyroxene (~5–7%, < 1 mm), and hornblende (< 3%, ~1–2 mm long). At least 4 individual lava flows crop out at Brown Knob, based on slight variations in phenocryst percentages, groundmass color, and erosional steps. These lavas form many of the topographic highs on the southwestern slope of the Terrill Mountains. The thickest stratigraphic section (≥90 m, top is eroded) in the quadrangle is exposed at the top of Brown Knob, the highest point in the map area. These lavas form many of the topographic highs on the southwestern slope of the Terrill Mountains. Age: 19.15±0.23 Ma ($^{40}Ar/^{39}Ar$, this study).

Tbkc Volcaniclastic conglomerates, breccias, and sandstone of Brown Knob (early Miocene) Multiple poorly-sorted, matrix-supported conglomerates and clast-supported breccias of primarily andesitic and dacitic clasts, ranging in thickness from ~5–10 m. Conglomerates and breccias are intercalated with ~1–2 m thick deposits of poorly-indurated, well- to moderately sorted, medium-grained, volcaniclastic sandstone with well-rounded gravel beds that commonly display crossbedding. The stratigraphically lowest breccia, as exposed at Brown Knob, is distinctive in its pebble to boulder size, angular to subangular clasts of dacite that contain euhedral phenocrysts of hornblende (~15–20%, up to 2 cm long) within a light gray to pinkish groundmass; ~200 m thick.

Tbka$_1$ Older basaltic andesite lavas of Brown Knob (early Miocene) Dark gray to reddish-brown, aphanitic basaltic to andesitic lavas commonly vesicular and scoriaceous. Flattened and slightly stretched vesicles in some flows locally define flow foliation planes. These basal flows of Brown Knob are thinner and less distributed in comparison to the younger andesitic flows; up to ~50 m thick in the central Terrill Mountains.

Tbp Plagioclase basalts (early Miocene to late Oligocene) Multiple dark gray to dark red, locally vesicular basaltic flows with intergranular plagioclase groundmass that contain distinctive large, platey, subhedral bytownite phenocrysts (~15–20%, ~1–2cm x 1–2cm x 1–3mm). Phenocrysts typically display a preferred orientation with long axes within the foliation planes. Preferred orientations of phenocrysts are commonly not observed or unidentifiable within vesicular sections. Crops out only in the northwest corner of the quadrangle; ~50 m thick.

Tvc Volcaniclastic conglomerates and breccias (late Oligocene) Very poorly sorted, subangular to subrounded, coarse sands to boulders of matrix-supported volcaniclastic deposits. A distinctive, very light gray, volcaniclastic, medium- to coarse-grained sandstone, ~3–5 m thick, lies directly above Tbpo. Tvc only crops out in the northwestern-most corner of the quadrangle. Though distinctive clasts of hornblende andesite of similar composition to clasts of a volcaniclastic breccia in the Brown Knob units are noted, the conglomerates and breccias are older and stratigraphically separated from Tbkc in the Brown Knob units by the younger plagioclase basalts (Tbp). No interfingering relationships between Tvc and Tbkc were observed, yet are possible in the subsurface. Up to ~30 m thick in the northern Terrill Mountains.

Tbpo Oldest plagioclase basalts (late Oligocene) One or two dark gray, basaltic lava flow(s) that contain distinctive large, platey, subhedral plagioclase phenocrysts (~15–20%, ~1–2cm x 1–2cm x 1–3mm), similar in percentage and size to phenocrysts indentified in the younger plagioclase basalts (Tbp). Phenocrysts typically display a preferred orientation with long axes within the foliation planes. Isolated outcrops were observed only in the northeasternmost corner of the quadrangle, stratigraphically below, and in contact with, the volcaniclastic sandstone of Tvc; ~40 m thick.

Tertiary intrusions

Tri Rhyolitic intrusion (early Miocene) Localized, flow-banded intrusion of felsic composition. Groundmass is light gray and contains phenocrysts of alkali feldspar (~7%, ~1–2 mm long), quartz (~5%, ~1 mm), and euhedral to subhedral biotite (~5%, ~1–2 mm). This unit displays an irregular contact with the country rock Tbkl and does not correlate with any lavas of Brown Knob. Crops out in the northern Terrill Mountains as an isolated and irregular body ~200 x 100 m thick.

Tdi Dacitic intrusions (early Miocene) Elongate and localized intrusions of intermediate composition. Aphanitic groundmass is medium-light gray and contains distinctive phenocrysts of euhedral hornblende (~7–8%, 2–5 mm long). Crops out in the northern Terrill Mountains as an isolated and elongate body ~200 x 50 m thick.

Tbi Basaltic intrusions (late Oligocene) Elongate and localized intrusions of mafic to intermediate composition. The intrusions are aphanitic and oriented subparallel to major right-lateral oblique-slip faults. Intrusions are similar in composition and texture to map unit Tb, but are not observed to crosscut Miocene units. Crops out as irregular and elongate bodies up to ~500 m long and up to ~100 m thick.

Thai Hornblende andesite intrusion (early Miocene) Localized andesite-dacite intrusion directly north-northeast of Brown Knob. Light purplish-gray trachytic groundmass, consisting of euhedral oligoclase laths (~0.1 mm); contains needle-like phenocrysts of subhedral to euhedral hornblende

(~1–2%, 1–3 mm long). Crops out directly north of Brown Knob as an isolated body ~500 m thick.

Ti Plagioclase hornblende intrusions, dikes, and sills (early Miocene) This regionally extensive unit intrudes Oligocene ignimbrites, units of Brown Knob, and faults in the form of dikes, sills, and irregular-shaped massive bodies. Porphyritic with light gray, interstitial plagioclase groundmass; contains phenocrysts of subhedral bytownite (~20%, ~2–3 mm), hornblende (~10%, ~2–7 mm), and biotite (~2–3%; 1–2 mm). The amounts of hornblende and biotite phenocrysts, and relative size of plagioclase phenocrysts, decrease near chilled margins and within relatively smaller volume intrusions. Crops out as dikes and sills ranging from 10s to 100s of meters thick and is emplace in the northern-central Terrill Mountains as large intrusive and sinuous bodies up to ~600 m thick and ~2 km long. Age: 22.67±0.15 Ma ($^{40}Ar/^{39}Ar$, this study).

Tiu Tertiary dikes, undivided (early Miocene) Aphanitic dikes that intrude small faults with little offset in the central Terrill Mountains, and have not been correlated to any other intrusions observed in the quadrangle. Dikes are <5–10 m thick and up to ~500 m long.

Oligocene ash-flow tuffs

Ttt Tuff of Toiyabe (late Oligocene) Light tan to reddish-brown, densely to moderately welded ash-flow tuff that contains phenocrysts of anhedral quartz (~10%, ~1–2 mm), subhedral sanidine (~10%, ~1–2 mm), andesine (~5%, ~1–2 mm long), euhedral biotite (~2–5%, 2–4 mm), and trace subhedral to euhedral sphene (~1%, <1 mm). Sphene is not as abundant as noted in other studies (e.g., Henry and John, 2013). Characteristics vary across map area. White and moderately flattened pumice fragments in lower sections of tuff contain ~1–2 mm long euhedral biotite. Abundance of pumice, which are commonly <1–2 cm long and have a low flattening ratio, if flattened at all, and decreases up section. The basal vitrophyre is ~1–2 m thick and not evident everywhere at base of section. ~120 m thick in the central Terrill Mountains. Age: 23.29±0.02 Ma ($^{40}Ar/^{39}Ar$, this study).

Ttu$_5$ Unknown tuff 5 (late Oligocene) Light green to light tan, poorly welded ash-flow tuff that contains phenocrysts of subhedral sanidine (~5–7%, ~1–2 mm) and quartz (~2%, ~1 mm). Lower section contains angular lithic clasts (~2–3%, ~3–6 mm) of jasper; these clasts commonly form lenses/pockets of up to 50% lithics. Unit is typically devoid of pumice fragments, but some outcrops locally display a preferential parting plane parallel to foliation. In several locations, the uppermost ~1–2 m (immediately below overlying Ttt) typically crops out as a crumbly, poorly consolidated, distinctive reddish-brown unit, inferred as a paleosol. The same uppermost section below Ttt in other locations is commonly characterized by development of a C soil horizon. Up to ~150 m thick in the northern Terrill Mountains.

Ttu$_4$ Unknown tuff 4 (late Oligocene) Peach to purplish, moderately welded ash-flow tuff that contains phenocrysts of subhedral sanidine (~10–15%, 1–2 mm), oligoclase (~5%, <1 mm), quartz (~10%, ~1 mm), and euhedral biotite (<1%, <1 mm). Unit contains abundant pumice fragments that are more flattened down section. Top of unit appears weathered and planar where exposed with a very clear and discrete contact with overlying unit. Weathered surfaces can appear lithophysal, where pumice fragments have been eroded. Relatively thin (<20 m) and discontinuous outcrops only observed in the central and southern Terrill Mountains.

Tgv Tuff of Gabbs Valley (late Oligocene) Densely welded ash-flow tuff that contains phenocrysts of subhedral sanidine (~5%, ~1–2 mm), andesine (<1%, <0.5 mm), quartz (~2–3%, ~0.5 mm), and biotite (~1–2%, ~1 mm), commonly containing abundant and highly stretched pumice (fiamme). Upper sections have fewer fiamme and are more purplish-brown; ~50–60 m thick. Age: 24.95±0.02 Ma ($^{40}Ar/^{39}Ar$, this study).

Ttu$_3$ Unknown tuff 3, undivided (late Oligocene) Light tan to light pink and purple, poorly welded ash-flow tuff that contains phenocrysts of sanidine (~7–10%, ~1–2 mm), oligoclase (~7%, ~1 mm), quartz (~3–5%, ~1 mm), and euhedral biotite (~2–3%, ~1 mm). Pumice are mostly sparse, and, where present, are small (~3–4 mm long) and moderately flattened. Unit is devoid of the extensive lithics present in Ttu$_2$ below. Up to ~170 m thick in the central Terrill Mountains.

Tec Tuff of Elevenmile Canyon (late Oligocene) Light tan to light pinkish-tan, moderately welded ash-flow tuff that contains phenocrysts of subhedral oligoclase (~15%, ~1 mm), sanidine (~10%, 1–2 mm), anhedral quartz (~3%, ~1 mm), and subhedral to euhedral biotite (~2%, 1–2 mm). White, highly-flattened pumice fragments (1–2 mm thick, ~20–30 mm long). Unit was observed in the northern Terrill Mountains; ~150 m thick. Age: 25.1 Ma (Henry and John, 2013).

Ttv Unknown tuff vitrophyre (late Oligocene) Densely welded, ash-flow tuff that contains phenocrysts of subhedral sanidine (~10%, ~1 mm), oligoclase (~5%, ~1–2 mm), quartz (~10%, ~1 mm), and biotite (~2%, ~1 mm). Thin (~10–20 m thick) and found only in northern Terrill Mountains.

Ttu$_2$ Unknown tuff 2 (late Oligocene) Light-green to light-tan, poorly welded ash-flow tuff that contains phenocrysts of sanidine (~5–7 %, ~1 mm), oligoclase (~5%, <1mm long), quartz (~5%, ~1mm), and biotite (trace). Some sections of tuff can be slightly darker yellowish-green and moderately-welded (< 2 m thick). Unit is distinctive in the quadrangle in its abundance of lithic clasts (mostly volcanic and cryptocrystalline quartz clasts, upwards of several centimeters in length and composing up to ~20% of unit in some locations). Small (~2–3 cm) devitrified fiamme are present in moderately welded sections. Outcrops in the

southwest part of the quadrangle, east of the Calico Hills, contain abundant petrified wood. Up to ~200 m thick in the central Terrill Mountains.

Tnh Nine Hill Tuff (late Oligocene) Densely welded ash-flow tuff that contains phenocrysts of subhedral sanidine (5%, ~1–2 mm), anorthoclase (<5%, ~1–2 mm), andesine (<<1%, <0.5 mm), and quartz (~1%, ~1 mm). Abundant pumice are highly stretched, and the rock is commonly rheomorphic. Up to ~40 m thick in the northern Terrill Mountains. Age: 25.44±0.02 Ma ($^{40}Ar/^{39}Ar$, this study).

Tmp Guild Mine Member of Mickey Pass Tuff (late Oligocene) Pink to reddish-pink and purple, densely to moderately welded ash-flow tuff that contains variable percentages of phenocrysts (~15–25%) of subhedral sanidine (~5–10%, ~1 mm long), oligoclase (~1%, <1 mm), quartz (~10%, ~1–2 mm), and biotite (~2–3%, ~1 mm). White, flattened pumice fragments, ranging from 5–30 mm long and 2–10 mm thick, form lineations parallel to compaction foliation. Outcrops only identified in the northern portion of the Terrill Mountains, where the tuff nonconformably overlies basement exposures at the northeastern range front. Other members of Mickey Pass Tuff may crop out in the map area but were not observed. Up to ~300 m thick in the northern Terrill Mountains. Age: 27.3 Ma (Henry and John, 2013).

Pre-Tertiary Rocks

JKg Gabbro (Cretaceous to Jurassic) Dark gray to greenish-black, phaneritic gabbro. Unit contains subhedral labradorite (~60–65%, ~1 mm long), anhedral orthopyroxene (~30–35%, 0.5–1 mm), and anhedral opaque minerals (~5%, commonly <0.5 mm). Outcrops of gabbro in the quadrangle are only exposed in the northernmost footwall of the fault bounding the northeast flank of the Terrill Mountains.

Jqd Quartz diorite (Jurassic) Medium gray, 'salt and pepper', phaneritic diorite. Unit contains euhedral to subhedral andesine (~35%, 1–2 mm), microcline (~25%, 1–2 mm), subhedral to anhedral hornblende (~25%, ~1–2 mm), anhedral interstitial quartz (~10–15%, < 1 mm), and anhedral biotite (<5%, <1mm). Diorite is only exposed in the northernmost footwall of the fault bounding the northeast flank of the Terrill Mountains.

Mzu Basement rocks, undivided (Mesozoic) Used for undivided basement outcrops and in cross sections, located between mapped JKg and Jqd, exposed in the footwall of the Benton Spring fault bounding the northeast flank of the Terrill Mountains. Unit may include some metavolcanic and/or metasedimentary rocks that do not crop out in map area.

ACKNOWLEDGMENTS

Research supported by the U.S. Geological Survey, National Cooperative Geologic Mapping Program, under USGS EDMAP program Agreement No. G13AC00106, 2013 and National Science Foundation grant EAR1419724. Significant appreciation is given to J. Faulds for assistance with grant writing and review of final EDMAP products and S. Wesnousky for his assistance in acquiring the NSF funding. Of important mention is the assistance of N. Hinz and the Cartography Support group of the Nevada Bureau of Mines and Geology who aided in transforming the collected field data into this final map. The views and conclusions contained in this document are those of the author and should not be interpreted as necessarily representing the official policies, either expressed or implied, of the U.S. Government.

REFERENCES

Bormann, J., Hammond, W.C., Kreemer, C., and Blewitt, G., 2016, Accommodation of missing shear strain in the central Walker Lane, western North America—constraints from dense GPS measurements: Earth and Planetary Science Letters, v. 440, p. 169–177, doi:10.1016/j.epsl.2016.01.015.

Briggs, R.W., and Wesnousky, S.G., 2004, Late Pleistocene fault slip rate, earthquake recurrence, and recency of slip along the Pyramid Lake fault zone, northern Walker Lane, United States: Journal of Geophysical Research, v. 109, n. B8, 16 p.

Carlson, C.W., 2014, Preliminary geologic map of the Terrill Mountains quadrangle, Churchill and Mineral counties, Nevada: Nevada Bureau of Mines and Geology Open-File Report 14-4, scale 1:24,000.

Carlson, C.W., 2017a, Preliminary geologic map of the Red Ridge area, Churchill and Mineral counties, Nevada: Nevada Bureau of Mines and Geology Open-File Report 17-2, scale 1:24,000, 7 p.

Carlson, C.W., 2017b, Kinematics and transfer mechanisms of strain accommodation at the transition between the northern and central Walker Lane, western Nevada: Reno, University of Nevada, Ph.D. dissertation, 220 p.

Carlson, C.W., Pluhar, C.J., Glen, J.M.G, and Farner, M.J., 2013, Kinematics of the west-central Walker Lane—Spatially and temporally variable rotations evident in the late Miocene Stanislaus Group: Geosphere, v. 9; no. 6; p. 1–22; doi:10.1130/GES00955.1.

Cashman, P.H., and Fontaine, S.A., 2000, Strain partitioning in the northern Walker Lane, western Nevada and northeastern California: Tectonophysics, v. 326, p. 111–130.

Deino, A.L., 1985, Stratigraphy, chemistry, K-Ar dating and paleomagnetism of the Nine Hill Tuff, California–Nevada, Part I, Miocene–Oligocene tuffs of Seven Lakes Mountain, California–Nevada, Part II: Berkeley, University of California, Ph.D. dissertation, 432 p.

Ekren, E. B., and Byers, F. M., Jr., 1984, The Gabbs Valley Range—a well-exposed segment of the Walker Lane in west-central Nevada, *in* Lintz, J., Jr., editor, Western geologic excursions, v. 4: Reno, Nevada, Geological Society of America Guidebook, Annual Meeting, 1984, p. 203–215.

Ekren, E.B., and Byers Jr., F. M., 1986, Geologic map of the Murphys Well, Pilot Cone, Copper Mountain, and Poinsettia Spring quadrangles, Mineral County, Nevada, U.S. Geological Survey Map, I-1576, scale 1:48,000.

Faulds, J.E., and Henry, C.D., 2008, Tectonic influences on the spatial and temporal evolution of the Walker Lane—an incipient transform fault along the evolving Pacific–North American plate boundary, *in* Spencer, J.E., and Titley, S.R., editors., Ores and orogenesis—Circum-Pacific tectonics,

geologic evolution, and ore deposits: Arizona Geological Society Digest 22, p. 437–470.

Faulds, J.E., and Perkins, M.E., 2007, Evidence for dextral shear along the western margin of the Carson Sink—the missing link between the central and northern Walker Lane, western Nevada: Geological Society of America Abstracts with Programs, v. 39, no. 4, p. 15.

Faulds, J.E., Henry, C.D., Hinz, N.H., Delwiche, B., and Cashman, P.H., 2004, Kinematic implications of new paleomagnetic data from the northern Walker Lane, western Nevada—counterintuitive anticlockwise vertical-axis rotation in an incipient dextral shear zone: EOS, American Geophysical Union, v. 85, no. 47, Abstract GP42A-08.

Faulds, J.E., Henry, C.D., Hinz, N.H., 2005, Kinematics of the northern Walker Lane—an incipient transform fault along the Pacific–North American plate boundary: Geology, v. 33, no. 6, p. 505–508.

Geissman, J.W, Van Der Voo, R., and Howard, K.L., Jr., 1982, A paleomagnetic study of the structural deformation in the Yerington district, Nevada: American Journal of Science, v. 282, p. 1042–1109.

Gromme, C.S., McKee, E.H., and Blake, M.C., Jr., 1972, Paleomagnetic correlations and potassium-argon dating of middle Cenozoic ash-flow sheets in the eastern Great Basin, Nevada and Utah: Geological Society of America Bulletin, v. 83, p. 1619–1638, doi: 10.1130/0016-7606(1972)83[1619:PCAPDO]2.0.CO;2.

Hardyman, R.F., McKee, E.H., Snee, L.W., Whitebread, D.H., 1992, The Camp Terrill and Dicalite Summit faults—two contrasting examples of detachment faults in the central walker Lane: Geological Society of Nevada Walker Lane Symposium Proceedings Volume, p. 93–113.

Henry, C.D., and Faulds, J.E., 2010, Ash-flow tuffs in the Nine Hill, Nevada, paleovalley and implications for tectonism and volcanism of the western Great Basin, USA: Geosphere,v. 6, p. 339–369, doi:10.1130/GES00548.1.

Henry, C.D., and John, D.A., 2013, Magmatism, ash-flow tuffs, and calderas of the ignimbrite flareup in the western Nevada volcanic field, Great Basin, USA: Geosphere, v. 9, no. 4, p. 951–1008,doi: 10.1130/GES00867.1.

Hinz, N.H., Faulds, J.E., and Oppliger, G.L., 2010, Preliminary geologic map of the Lee-Allen geothermal area, Churchill County, Nevada: Nevada Bureau of Mines and Geology Open-File Report 10-6, scale 1:24000 (with 1:12000 inset).

John, D.A., 1995, Tilted middle Tertiary ash-flow calderas and subjacent granitic plutons, southern Stillwater Range, Nevada—cross-sections of an Oligocene igneouscenter: Geological Society of America Bulletin,v. 107, p. 180–200.

Kuiper, K.F., Deino, A., Hilgen, F.J., Krijgsman, W., Renne, P.R., and Wijbrans, J.R., 2008, Synchronizing rock clocks of earth history: Science, v. 320, p. 500–504.

Lee, J., Stockli, D.F., Owen, L.A., Finkel, R.C., and Kislitsyn, R., 2009, Exhumation of the Inyo Mountains, California—implications for the timing of extension along the western boundary of the Basin and Range Province and distribution of dextral fault slip rates across the eastern California shear zone: Tectonics, v. 28, TC1001, doi:10.1029/2008TC002295.

Minn, K., Mundil, R., Renne, P.L., and Ludwig, K.R., 2000, A test for systematic errors in $^{40}Ar/^{39}Ar$ geochronology through comparison with U/Pb analysis of a 1.1-Ga rhyolite: Geochimica et Cosmochimica Acta, v. 64, p. 73–98.

Oldow, J.S., Aiken, C.L.V., Hare, J.L., Ferguson, J.F., and Hardyman, R.F., 2001, Active displacement transfer and differential block motion within the central Walker Lane, western Great Basin: Geology, v. 29, no. 1, p. 19–22.

Reheis, M., 1999, Extent of pleistocene lakes in the western Great Basin: U.S. Geological Survey Miscellaneous Field Studies Map MF-2323, scale 1:800,000.

Stewart, J.H., 1988, Tectonics of the Walker Lane belt, western Great Basin: Mesozoic and Cenozoic deformation in a zone of shear, *in* Ernst, W. G., editor, Metamorphism and crustal evolution of the western United States: Prentice Hall, Englewood Cliffs, New Jersey, p. 681–713.

Taylor, J.R., 1982, An introduction to error analysis—the study of uncertainties in physical measurements: University Science Books, Mill Valley, California, 270 p.

Wesnousky, S.G., 2005, Active faulting in the Walker Lane: Tectonics, v. 24, p. 1–35, doi: 10.1029/2004TC001645.

Wesnousky, S.G., Bormann, J.M., Kreemer, C., Hammond, W.C., and Brune, J.N., 2012, Neotectonics, geodesy, and seismic hazard in the northern Walker Lane of western North America—thirty kilometers of crustal shear and no strike slip?: Earth and Planetary Science Letters, v. 329–330, p. 133–140, doi: 10.1016/j.epsl.2012.02.018.

Suggested Citation:

Carlson, C.W., 2018, Geologic map of the Terrill Mountains quadrangle, Churchill and Mineral counties, Nevada: Nevada Bureau of Mines and Geology Map 187, scale 1:24,000, 16 p.

APPENDIX A

$^{40}Ar/^{39}Ar$ Analytical Methods and Results

Samples from three Oligocene ash-flow tuffs, an early-Miocene intrusion, early-Miocene lava, and late-Miocene lava were analyzed by the New Mexico Geochronology Research Laboratory in the summer of 2016. Results are used to support correlations to previously-dated and regionally-extensive Oligocene ash-flow tuffs and elucidate the timing and evolution of Neogene deformation in the Terrill Mountains region. Single crystal analyses of sanidine were completed on ash-flow tuffs (table 1A). Step-heated, multigrain, analyses of plagioclase separates and groundmass concentrate were completed on Miocene lavas and intrusion (table 1A). $^{40}Ar/^{39}Ar$ sample locations and ages are included on the map of the Terrill Mountains quadrangle.

Mineral separates and monitors (Fish Canyon Tuff sanidine, 28.201 Ma, Kuiper et al., 2008) were loaded into aluminum discs and irradiated for 16 hours at the USGS TRIGA reactor in Denver, Colorado. Irradiated samples were analyzed at New Mexico Geochronology Research Laboratory. Individual crystals of sanidine and Fish Canyon Tuff sanidine monitors were fused with a Photon Machines CO_2 laser and analyzed with a Thermo Argus VI mass spectrometer. Small (6–8 mg) multigrain samples of groundmass and plagioclase were step-heated with a Photon Machines Diode laser and analyzed with a Thermo Helix MC Plus mass spectrometer. Abbreviated analytical methods for the dated samples are given in table 1A. The age results are summarized in table 1A and the argon isotopic data are given in tables 2A and 3A.

Table 1A. Summary of $^{40}Ar/^{39}Ar$ results and analytical methods

Sample #	Irradiation	Mineral	Age Analysis	Steps/ Analyses	Age	±2σ	MSWD
CC15-021-3	283	groundmass concentrate	bulk step-heat	3	5.79	0.06	6.4
MBK06-4	283	plagioclase	bulk step-heat	10	19.15	0.23	6.8
CC15-021-1	283	plagioclase	bulk step-heat	8	22.67	0.15	2.2
NTM-093-1	283	sanidine	laser fusion	10	23.29	0.02	18.5
STM04-2	283	sanidine	laser fusion	11	24.95	0.02	7.8
PMA01-2	283	sanidine	laser fusion	9	25.44	0.02	9.9
CC15-019-2	283	plagioclase	bulk step-heat	-	-	-	-

Notes: Sample preparation and irradiation: Minerals separated with Franz Magnetic and hand-picking techniques. Samples in NM-283 irradiated in a machined Aluminum tray for 16 hours in C.T. position, USGS TRIGA, Denver, Colorado. Neutron flux monitor Fish Canyon Tuff sanidine (FC-2). Assigned age = 28.201 Ma (Kuiper et al., 2008).

Instrumentation: Total fusion analyses performed on an Argus VI mass spectrometer on line with automated all-metal extraction system. Step-heat analyses performed on a Helix MCPlus mass spectrometer on line with automated all-metal extraction system. Multi-collector configuration: ^{40}Ar-H1, ^{39}Ar-Ax, ^{38}Ar-L1, ^{37}Ar-L2, ^{36}Ar-CDD

Flux monitors fused with a Photon Machines Inc. CO_2 laser. Groundmass concentrate and glass step-heated with a Photon Machine Inc. Diode laser.

Analytical parameters: Sensitivity for the Helix MCPlus with the Diode laser (step-heated samples) is 3.0 e-16 moles/fA. Sensitivity for the Argus VI with the CO_2 laser (fused monitors) is 4.62 e-17 moles/fA. Typical system blank and background was 83.9, 1.32, 0.499, 0.382, 0.320 x 10–18 moles at masses 40, 39, 38, 37 and 36, respectively for the laser analyses. J-factors determined by CO_2 laser-fusion of 6 single crystals from each of 8 radial positions around the irradiation tray. Decay constants and isotopic abundances after Minn et al., (2000).

Table 2A. Analytical data

ID	$^{40}Ar/^{39}Ar$	$^{37}Ar/^{39}Ar$	$^{36}Ar/^{39}Ar$ (x 10^{-15}mol)	^{39}ArK (x 10^{-15}mol)	K/Ca	$^{40}Ar^{*}$ (%)	Age (Ma)	±1σ (Ma)
NTM-093-1, san J=0.0039094±0.02%, D=1±0, NM-283G, Lab#=64989								
*5	3.201	0.0068	0.0490	2.960	75.3	99.6	22.62	0.01
15	3.271	0.0084	0.0073	2.632	60.7	100.0	23.20	0.01
10	3.290	0.0051	0.0534	2.456	99.3	99.5	23.24	0.01
9	3.299	0.0045	0.0739	1.697	113.3	99.3	23.25	0.01
13	3.277	0.0077	0.0000	2.683	65.9	100.0	23.26	0.01
14	3.282	0.0078	0.0105	2.822	65.4	99.9	23.27	0.01
12	3.281	0.0076	0.0052	3.671	67.6	100.0	23.27	0.01
7	3.302	0.0053	0.0722	1.940	95.4	99.4	23.28	0.01
3	3.296	0.0062	0.0469	4.301	82.2	99.6	23.29	0.01
4	3.294	0.0075	0.0288	5.681	68.2	99.8	23.31	0.01
6	3.294	0.0062	0.0274	5.841	82.3	99.8	23.32	0.01
*8	3.641	-0.0200	0.7095	0.161	-	94.2	24.33	0.16
Mean age ± 2σ		**n=10**	**MSWD=18.53**		**80.0±35.3**		**23.29**	**0.02**
PMA01-2, san, J=0.003908±0.02%, D=1±0, NM-283G, Lab#=64990								
1	3.624	0.0319	0.1471	2.995	16.0	98.9	25.40	0.01
11	3.626	0.0337	0.1548	3.428	15.1	98.8	25.40	0.01
3	3.626	0.0350	0.1494	2.967	14.6	98.9	25.41	0.01
14	3.631	0.0529	0.1696	2.830	9.6	98.7	25.42	0.01
6	3.616	0.0281	0.1065	2.835	18.1	99.2	25.43	0.01
4	3.667	0.0379	0.2789	4.294	13.5	97.8	25.43	0.01
5	3.626	0.0511	0.1431	1.668	10.0	98.9	25.44	0.02
15	3.625	0.0436	0.1333	5.517	11.7	99.0	25.45	0.01
9	3.656	0.0640	0.2323	3.780	8.0	98.3	25.47	0.01
7	3.620	0.0679	0.1086	5.445	7.5	99.3	25.47	0.01
10	3.639	0.0477	0.1663	5.048	10.7	98.8	25.48	0.01
13	3.891	0.0348	1.0130	5.618	14.6	92.4	25.49	0.01
2	3.645	0.0455	0.1437	4.520	11.2	98.9	25.56	0.01
8	3.620	0.0428	0.0448	3.179	11.9	99.7	25.59	0.01
12	3.677	0.0321	0.2026	1.958	15.9	98.4	25.66	0.01
Mean age ± 2σ		**n=12**	**MSWD=9.92**		**12.5±6.7**		**25.44**	**0.02**

Table 2A (cont.). Analytical data

ID	$^{40}Ar/^{39}Ar$	$^{37}Ar/^{39}Ar$	$^{36}Ar/^{39}Ar$ (x 10^{-15}mol)	^{39}ArK (x 10^{-15}mol)	K/Ca	$^{40}Ar^{*}$ (%)	Age (Ma)	±1σ (Ma)
STM04-2, san, J=0.0039075±0.02%, D=1±0, NM-283G, Lab#=64991								
12	3.731	0.0142	0.7527	2.646	36.0	94.1	24.88	0.02
3	3.560	0.0262	0.1616	2.575	19.5	98.7	24.91	0.01
4	3.532	0.0199	0.0606	3.608	25.6	99.5	24.93	0.01
6	3.559	0.0199	0.1476	6.141	25.7	98.8	24.93	0.01
1	3.557	0.0221	0.1345	3.417	23.1	98.9	24.94	0.01
7	3.541	0.0200	0.0747	2.947	25.5	99.4	24.95	0.01
11	3.623	0.0213	0.3418	3.071	24.0	97.3	24.98	0.01
2	3.566	0.0221	0.1478	3.276	23.0	98.8	24.98	0.01
14	3.624	0.0200	0.3429	3.237	25.5	97.2	24.98	0.01
9	3.858	0.0198	1.1330	1.208	25.8	91.3	24.99	0.04
5	3.542	0.0299	0.0566	1.630	17.0	99.6	25.01	0.02
*15	3.632	0.0115	0.2753	2.892	44.4	97.8	25.17	0.01
*13	4.085	0.0250	1.5980	1.195	20.4	88.5	25.62	0.04
*8	3.713	0.0215	0.1064	2.569	23.8	99.2	26.10	0.01
*10	17.610	0.0195	0.6567	1.665	26.2	98.9	120.45	0.05
Mean age ± 2σ		**n=11**	**MSWD=7.81**		**24.6±9.4**		**24.95**	**0.02**

Notes: Isotopic ratios corrected for blank, radioactive decay, and mass discrimination, not corrected for interfering reactions. Errors quoted for individual analyses include analytical error only, without interfering reaction or J uncertainties. Mean age is weighted mean age of Taylor (1982). Mean age error is weighted error of the mean (Taylor, 1982), multiplied by the root of the MSWD where MSWD>1, and also incorporates uncertainty in J factors and irradiation correction uncertainties.

Decay constants and isotopic abundances after Minn et al., (2000).

* symbol preceding sample ID denotes analyses excluded from mean age calculations.

Ages calculated relative to FC-2 Fish Canyon Tuff sanidine interlaboratory standard at 28.201 Ma

Decay Constant (LambdaK (total)) = 5.463e-10/a

Correction factors:

$(^{39}Ar/^{37}Ar)Ca$ = 0.0006928 ± 5e-06

$(^{36}Ar/^{37}Ar)Ca$ = 0.0002702 ± 0

$(^{38}Ar/^{39}Ar)K$ = 0.01261

$(^{40}Ar/^{39}Ar)K$ = 0.007439 ± 0.000146

Table 3A. $^{40}Ar/^{39}Ar$ Analytical data

ID	Power (Watts)	$^{40}Ar/^{39}Ar$	$^{37}Ar/^{39}Ar$	$^{36}Ar/^{39}Ar$	$^{39}Ar_K$ (x 10^{-15} mol)	K/Ca	$^{40}Ar^*$ (%)	^{39}Ar (%)	Age (Ma)	±1σ (Ma)
CC15-019-2, plag, 5.87 mg, J=0.0039069±0.02%, IC=1.057846±0.0011235, NM-283G, Lab#64992-01, Helix MCPlus										
*A	2.0	5.933	9.902	6.572	6.6	0.052	80.6	18.7	34.06	0.09
*B	3.0	4.610	10.440	3.546	5.8	0.049	95.4	35.2	31.34	0.08
*C	4.0	4.079	11.670	3.455	3.2	0.044	97.8	44.4	28.49	0.11
*D	6.0	4.265	11.380	3.723	3.0	0.045	95.5	52.8	29.08	0.12
*E	7.0	4.024	11.900	3.515	1.8	0.043	97.8	57.7	28.11	0.18
*F	8.0	4.098	11.580	3.852	1.5	0.044	94.8	61.9	27.74	0.20
*G	10.0	4.304	10.860	3.559	1.7	0.047	95.7	66.6	29.39	0.19
*H	12.0	6.696	9.058	9.108	1.7	0.056	70.6	71.3	33.66	0.25
*I	15.0	3.863	10.680	3.591	8.1	0.048	94.6	94.1	26.10	0.06
*J	20.0	4.436	11.220	3.902	1.3	0.045	94.2	97.9	29.82	0.24
*K	25.0	6.848	6.054	3.175	0.7	0.084	93.4	100.0	45.30	0.51
Integrated age ± 2σ			n=11		35.4	0.048		K2O=0.59	30.15	0.08
CC15-021-1, plag, 5.8 mg, J=0.0039069±0.02%, IC=1.057846±0.0011235, NM-283G, 64993-01, Helix MCPlus										
*A	2.0	117.7	10.70	388.8	1.6	0.048	3.1	6.0	26.35	1.47
*B	3.0	4.643	10.28	8.101	6.7	0.050	66.1	31.3	21.93	0.09
*C	4.0	3.147	10.29	2.980	3.6	0.050	98.1	45.0	22.06	0.09
D	6.0	3.174	10.38	2.949	2.5	0.049	98.7	54.6	22.37	0.12
E	7.0	3.125	10.27	2.724	1.2	0.050	100.5	59.1	22.43	0.21
F	8.0	3.129	10.18	2.663	1.0	0.050	100.8	62.9	22.54	0.26
G	10.0	3.255	9.938	3.008	1.3	0.051	97.1	68.0	22.56	0.21
H	12.0	3.213	9.937	2.723	1.2	0.051	99.7	72.4	22.86	0.22
I	15.0	3.173	9.839	2.562	0.9	0.052	100.9	75.6	22.86	0.28
J	20.0	3.275	9.822	2.684	0.8	0.052	99.8	78.5	23.32	0.33
K	25.0	3.274	9.799	2.936	5.7	0.052	97.4	100.0	22.77	0.07
Integrated age ± 2σ			n=11		26.4	0.050		K2O=0.45	22.62	0.20
Plateau ±2σ	**steps D-K**		**n=8**	**MSWD=2.25**	**14.5**	**0.051±0.002**		**55**	**22.67**	**0.15**
Isochron ±2σ	steps A-K		n=11	MSWD=9.95		$^{40}Ar/^{36}Ar$= 296.4±3.5			22.42	0.25

Table 3A (cont.). $^{40}Ar/^{39}Ar$ Analytical data

ID	Power (Watts)	$^{40}Ar/^{39}Ar$	$^{37}Ar/^{39}Ar$	$^{36}Ar/^{39}Ar$	$^{39}Ar_K$ (x 10^{-15} mol)	K/Ca	$^{40}Ar^*$ (%)	^{39}Ar (%)	Age (Ma)	±1σ (Ma)
MBK06-4, plag, 6.08 mg, J=0.0039076±0.02%, IC=1.057846±0.0011235, NM-283G, Lab#=64994-01, Helix MCPlus										
*A	2.0	408.2	12.37	1368.1	0.4	0.041	1.2	1.8	35.36	5.33
B	3.0	3.715	12.15	6.978	2.7	0.042	70.6	12.8	18.78	0.16
C	4.0	2.649	13.13	3.645	2.4	0.039	98.9	22.6	18.77	0.13
D	6.0	2.749	13.51	4.063	2.4	0.038	95.6	32.3	18.82	0.13
E	7.0	2.654	13.69	3.827	1.5	0.037	98.6	38.3	18.75	0.18
F	8.0	2.695	13.51	4.005	1.1	0.038	96.1	43.0	18.56	0.22
G	10.0	2.665	13.57	3.836	1.1	0.038	98.1	47.4	18.74	0.23
H	12.0	3.864	13.71	7.532	0.9	0.037	70.7	51.1	19.58	0.31
I	15.0	2.689	13.49	3.561	1.0	0.038	100.9	55.1	19.44	0.26
J	20.0	2.784	13.49	3.914	1.0	0.038	97.2	59.1	19.38	0.25
K	25.0	3.204	13.59	5.329	9.9	0.038	84.7	100.0	19.45	0.06
Integrated age ± 2σ			n=11		24.2	0.038		K2O=0.39	19.42	0.21
Plateau ±2σ	**steps B-K**		**n=10**	**MSWD=6.80**	**23.8**	**0.038±0.003**		**98.2**	**19.15**	**0.23**
Isochron ±2σ	steps A-K		n=11	MSWD=6.68		$^{40}Ar/^{36}Ar$= 297.4±2.8			19.14	0.23
CC15-021-3, gm, 8.23 mg, J=0.0039225±0.02%, IC=1.031848±0.0003675, NM-283C, Lab#=64204-02, Helix MCPlus										
*A	0.5	7.743	0.2454	23.98	6.4	2.1	8.7	2.6	4.8	0.13
B	0.8	2.955	0.4804	7.373	26.2	1.1	27.4	13.4	5.8	0.04
C	1.3	1.908	0.6681	3.863	55.8	0.76	42.8	36.3	5.83	0.02
D	1.6	1.703	0.7262	3.229	41.8	0.70	47.2	53.5	5.73	0.02
*E	1.9	2.023	0.8080	4.422	30.5	0.63	38.4	66	5.55	0.03
*F	2.2	2.757	0.8993	7.029	21.3	0.57	27.1	74.8	5.34	0.04
*G	3.0	4.015	1.244	11.27	26.0	0.41	19.4	85.4	5.57	0.04
*H	5.0	5.052	1.578	14.74	19.6	0.32	16.2	93.5	5.86	0.06
*I	7.0	5.150	1.470	15.03	5.6	0.35	15.9	95.8	5.87	0.11
*J	10.0	5.588	1.735	16.38	10.3	0.29	15.7	100	6.3	0.09
Integrated age ± 2σ			n=10		243.6	0.58		K2O=2.90	5.70	0.02
Plateau ±2σ	**steps B-D**		**n=3**	**MSWD=6.43**	**123.9**	**0.806±0.385**		**50.9**	**5.79**	**0.06**
Isochron ±2σ	steps A-J		n=10	MSWD=35.45		$^{40}Ar/^{36}Ar$= 296.4±3.5			5.74	0.24

Notes (Table 3A): Isotopic ratios corrected for blank, radioactive decay, and mass discrimination, not corrected for interfering reactions. Errors quoted for individual analyses include analytical error only, without interfering reaction or J uncertainties. Integrated age calculated by summing isotopic measurements of all steps. Integrated age error calculated by quadratically combining errors of isotopic measurements of all steps. Plateau age is inverse-variance-weighted mean of selected steps. Plateau age error is inverse-variance-weighted mean error (Taylor, 1982) times root MSWD where MSWD>1. Plateau error is weighted error of Taylor (1982).

Decay constants and isotopic abundances after Minn et al. (2000)

* symbol preceding sample ID denotes analyses excluded from plateau age calculations.

Weight percent K2O calculated from ^{39}Ar signal, sample weight, and instrument sensitivity.

Ages calculated relative to FC-2 Fish Canyon Tuff sanidine interlaboratory standard at 28.201 Ma

Decay Constant (LambdaK (total)) = 5.463e-10/a

Correction factors:

$(^{39}Ar/^{37}Ar)Ca$ = 0.0006928 ± 0.000005

$(^{36}Ar/^{37}Ar)Ca$ = 0.0002702 ± 0.0000005

$(^{38}Ar/^{39}Ar)K$ = 0.01261

$(^{40}Ar/^{39}Ar)K$ = 0.007439 ± 0.000146